Absolute photoionization cross sections of the Cs $7D_{3/2}$ level measured by use of fluorescence reduction

K. D. Bonin, M. Gatzke, C. L. Collins, and M. A. Kadar-Kallen
Department of Physics, Princeton University, Princeton, New Jersey 08544
(Received 30 January 1989)

A simple technique for measuring absolute photoionization cross sections σ of excited atoms has been applied to the $7D_{3/2}$ level in Cs. Past experiments on excited-state cross sections have relied on measurements of the total number of ions or photoelectrons produced by photoionization to deduce σ. Our technique is novel in that it utilizes the simple measurement of the reduction in the excited-atom fluorescence due to photoionization to find σ. We report measurements of cross sections at six different photon energies.

I. INTRODUCTION

Recently there has been great interest in photoionization from excited states. From a fundamental atomic-physics standpoint photoionization-cross-section measurements are useful as tests of atomic theory. For example, past theoretical calculations[1-3] have indicated that Cooper minima in the photoionization cross section of excited levels are more numerous than for the ground states. Predictions of the presence and location of these minima, which occur due to cancellations from equal negative and positive contributions to the dipole matrix element, are sensitive to the wave functions used in the calculation. In some cases it is important to account for electron-electron correlations and core-polarization effects in the wave functions used to calculate cross sections and photoelectron angular distributions.[4] Only a small number of measurements of excited-state photoionization cross sections have been reported in the literature.[5-9] A recent review of excited-state photoionization can be found in the work of Wuilleumier *et al.*[10] A complete discussion of the theory of atomic photoionization measurements is given by Jacobs.[11]

Applications and techniques that rely on excited-state photoionization processes have also generated interest in measurements of corresponding cross sections. Examples include production of spin-polarized electrons using the Fano effect[12] and laser isotope separation, which usually involves multiphoton-ionization processes. Note, however, that the application to laser isotope separation is focused on autoionizing states.

Alkali-metal-atom photoionization studies are of interest because the alkali metals, having a single valence electron, are the simplest atoms to understand. Cesium is the most interesting of the alkali metals because electron-electron correlations, the spin-orbit interaction, and core-polarization effects are largest for this atom. In particular, various calculations have predicted multiple minima in the photoionization cross sections of the Cs *nd* levels.[3,13] Disagreement exists as to the number and location of such minima. For example, predictions about the Cs 9*d* photoionization dipole matrix elements include either two or three minima (see Avdonina *et al.*[13] and Lahiri and Manson[3]). For the Cs 6*d* level, after experimental observations of photoionization cross sections[8] showed the absence of a predicted minimum[14] near $\lambda \simeq 460$ nm, further calculations were performed using different wave functions that placed the new calculated first minimum at $\lambda \simeq 100$ nm for this level.[15] There exists a need for more data, particularly for Cs, and for new techniques to measure excited-state photoionization cross sections.

Here we report on a new technique for measuring photoionization cross sections σ of excited atoms. The method has been applied to the $7D_{3/2}$ level in cesium to obtain the first measurements of σ for this level. Cross sections were measured at six different photon energies. Past experiments on excited-state cross sections have generally relied on measurements of the total number of ions or photoelectrons produced by photoionization to deduce σ. Our technique is novel in that it utilizes a simple measurement of the reduction in the excited-atom fluorescence due to photoionization to find σ. A related technique for determining photoionization cross sections that combines a measurement of fluorescence reduction and the lifetime of the excited level was proposed by Gilbert *et al.*[9] However, this is the first report of a measurement using a fluorescence technique.

A reduced fluorescence technique was recently applied to core-excited levels of neutral rubidium to determine the position and linewidth of metastable lines.[16] A laser was used to transfer atoms from core-excited levels to autoionizing levels, thereby reducing the fluorescence of the core-excited level. From the linewidth measurement and a measurement of the transfer laser saturation energy density at line center, a transition oscillator strength could be determined. This method only applies to the measurement of autoionizing states, whereas the technique reported here applies to continuum states in general.

II. THEORY

An energy-level diagram showing the relevant physical processes (as applied to Cs) is given in Fig. 1. Excited-state atoms are initially produced by some means—

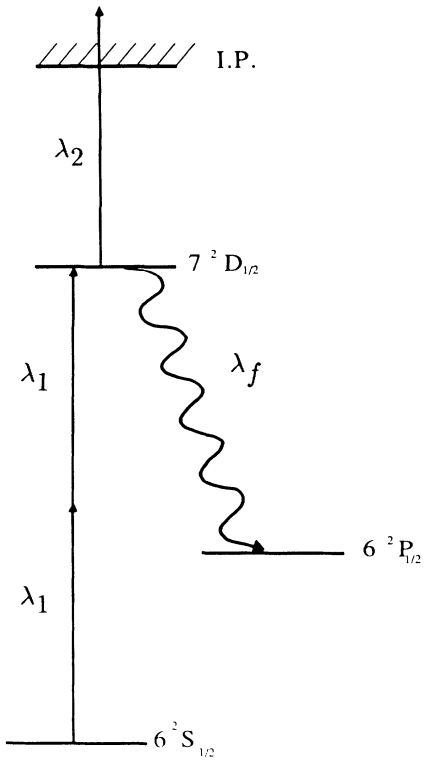

FIG. 1. Energy-level diagram showing relevant physical processes that are used to measure the photoionization cross section of excited states by fluorescence reduction. This diagram illustrates the important processes for the case of Cs reported here. Cesium atoms are excited to the $7D_{3/2}$ level by resonant two-photon absorption of light at $\lambda_1=767$ nm. Light at λ_2 photoionizes some of the excited atoms resulting in a reduction of the fluorescence at $\lambda_f=672$ nm. The ionization potential (IP) for the Cs $7D_{3/2}$ level is 0.662 eV.

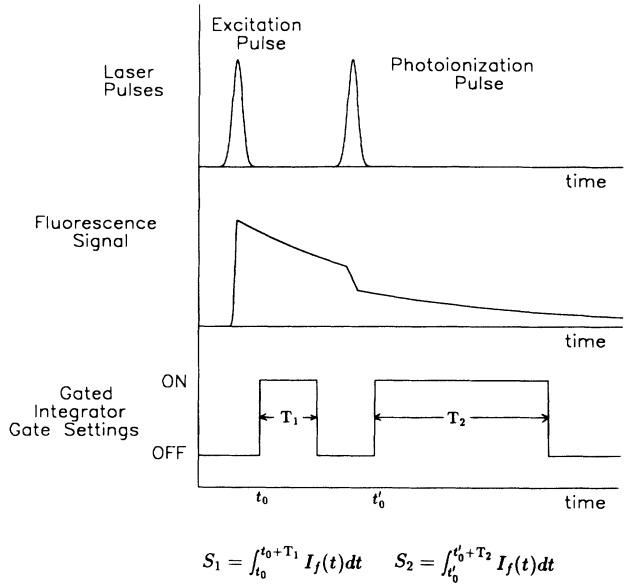

FIG. 2. Timing sequence for measuring photoionization cross sections by a reduction in fluorescence. The exciting and photoionizing laser pulses are shown at the top. The middle curve shows the fluorescence produced as the atoms decay from the initial excited level to a lower-lying level. The photoionization pulse causes a decrease in fluorescence due to removal of atoms from the excited fluorescing state. The bottom plot shows the gate settings or integration times for integrating the fluorescence before (interval T_1) and after (interval T_2) the photoionizing pulse is applied. The signal S_1 is used as a normalization for the signal S_2. We note that the integrations are performed using two independent gated integrators.

in our case by absorption of photons from a dye laser (pulsewidth = 3 ns) tuned to the $6S_{1/2}\rightarrow 7D_{3/2}$ two photon transition at $\lambda_1=767$ nm. The excited atoms then begin to radiatively decay with mean lifetime τ. We temporally integrate the fluorescence in one of the lines (wavelength λ_f) until a second photoionizing laser pulse is incident on the atoms. This second laser (wavelength λ_2, pulsewidth Δt_2 with $\Delta t_2 \ll \tau$) decreases the number of fluorescing atoms by photoionization. We then integrate the subsequent fluorescence for a few lifetimes. A timing diagram showing the sequence of laser pulses and integrated fluorescence signals is given in Fig. 2.

The integrated signal before photoionization, which we denote S_1, is obtained by integrating the fluorescence at λ_f for a time $T_1 \lesssim \tau/3$. This signal serves as a normalization to the integrated signal S_2 that is collected after the photoionization laser pulse has ended. The integration time for S_2 is typically several lifetimes ($T_2 \simeq 3\tau$). The normalization of S_2 by S_1 to form the ratio $R=S_2/S_1$ is important in order to significantly reduce shot-to-shot fluctuations in the fluorescent intensity due to variations in laser power. The need for this is especially acute in our case since the excitation process is nonlinear. We measure the ratio R as a function of the fluence F (in units of energy/area) of the photoionizing laser. The relationship between R and F can be found by considering the fundamental relation for the rate of change of fluorescing atoms as a function of the photoionizing laser intensity $I_2(t)$. This is given by the rate equation (we discuss coherences later)

$$\frac{dN(t)}{dt}=-N(t)\left[\sigma\frac{I_2(t)}{h\nu_2}+\frac{1}{\tau}\right], \tag{1}$$

where $N(t)$ is the number of atoms in the excited level at time t, σ is the frequency-dependent photoionization cross section, $I_2/h\nu_2$ is the incident photoionization-laser photon flux. From this it follows that

$$N(t)=N_0\exp-\left[\frac{\sigma}{h\nu_2}\int_{t_0}^{t}I_2(t')dt'+\frac{t-t_0}{\tau}\right]. \tag{2}$$

Here $t=t_0$ corresponds to any time after the excitation process and before the photoionization laser pulse and N_0 is the number of excited atoms present at this time. We assume the photoionization laser pulse is very short compared to the excited-state lifetime ($\Delta t_2 \ll \tau$). Thus, for times later than the photoionization pulse with $t \gg \Delta t_2$ and assuming t_0 is chosen to be significantly earlier than the passage of the second laser pulse, then we can ap-

proximate the last relation by

$$N(t)=N_0\left[\exp\left[-\frac{\sigma}{h\nu}F\right]\right]\left[\exp\left[-\frac{t-t_0}{\tau}\right]\right], \quad (3)$$

where

$$\int_{t_0}^{t} I(t')dt' \simeq \int_{-\infty}^{\infty} I(t')dt' \equiv F . \quad (4)$$

Note that we have dropped the subscript 2 as a label for quantities relating to the photoionization laser pulse. The fluorescent intensity $I_f(t)$ reaching the detector at a time t is given by

$$I_f(t)=\frac{\beta\hbar\omega_f}{A_d}\frac{\Delta\Omega}{4\pi}\frac{N(t)}{\tau}\equiv C\frac{N(t)}{\tau} , \quad (5)$$

where β is the branching ratio for the chosen fluorescence line, $\hbar\omega_f$ is the energy in a single photon, A_d is the detector area, and $\Delta\Omega/4\pi$ is the solid-angle fraction occupied by the detector. From this relation we can calculate expressions for the time-integrated signals S_1 and S_2. For the fluorescence signal integrated for a time T_1 before the photoionization pulse we get, by substituting (3) into (5) with $F=0$ and integrating

$$S_1=\int_{t_0}^{t_0+T_1} I_f(t)dt=\gamma_1 N_0 , \quad (6)$$

where $\gamma_1=G_1C(1-e^{-T_1/\tau})$ is a constant. The quantity G_1 represents the gated integrator gain. Likewise, for the integrated signal S_2 after photoionization we get (the integration begins at time t_0' and the integration time is T_2)

$$S_2=\int_{t_0'}^{t_0'+T_2} I_f(t)dt=\gamma_2 N_0\left[\exp\left[-\frac{\sigma}{h\nu}F\right]\right] , \quad (7)$$

where

$$\gamma_2=G_2C(e^{(t_0-t_0')/\tau}-e^{(t_0-t_0'-T_2)/\tau})$$

is a constant. The quantity G_2 represents the second gated integrator gain. From (6) and (7) we can form the ratio

$$R(F)\equiv\frac{S_2}{S_1}=A_0\exp\left[-\frac{\sigma}{h\nu}F\right] , \quad (8)$$

where $A_0=\gamma_2/\gamma_1$ is a parameter that depends on the integration times T_1 and T_2 and on the gain of the gated integrator amplifiers. From (8) it can be seen that by measuring R as a function of the photoionization laser fluence F (for a fixed frequency $h\nu$), the photoionization cross section σ can be determined. Notice that a set of data consisting of R versus F can be fitted by the expression (8) with only *one* free adjustable parameter, σ. The constant A_0 is obtained from the data by assigning it the value $A_0=R(F=0)$.

There are several aspects of the simple model above that must be discussed in more detail due to their dependences on experimental conditions. The first concerns the exact meaning of the photoionization cross section σ. For the measurements reported here we used the Cs $7D_{3/2}$ level which has four different magnetic quantum number sublevels, $|m_j\rangle\in\{\pm|\frac{3}{2}\rangle,\pm|\frac{1}{2}\rangle\}$. The azimuthal quantum number m_j is defined by

$$J_z|m_j\rangle=m_j|m_j\rangle , \quad (9)$$

where J_z is the z projection of the electronic angular-momentum operator. Here we assume J is a good quantum number and so hyperfine structure is ignored. From elementary perturbation theory[17] the following expression for the total photoionization cross section of a given sublevel can be written:

$$\sigma(b;aq)=4\pi^2\frac{e^2m_e}{\hbar^2}\frac{k}{q}\sum_{\lambda,\mu,m_s}|\langle b|\hat{\epsilon}\cdot\mathbf{D}|aq\lambda\mu m_s\rangle|^2 , \quad (10)$$

where $|b\rangle$ is the wave function of the excited atom, and $|aq\lambda\mu m_s\rangle$ refers to the wave function of the ion core and electron. The quantity m_s corresponds to the photoelectron's z component of spin, $\mathbf{q}$ is the wave vector of the electron, $\mathbf{k}$ and $\hat{\epsilon}$ are the absorbed photon's wave vector and unit polarization vector, respectively, and m_e is the electron mass. The quantity $\mathbf{D}$ is the electric dipole moment of the atom, i.e., $\mathbf{D}=\sum_i e\mathbf{r}_i$, where $\mathbf{r}_i$ is the position vector of the ith electron. The spatial part of the photoelectron wave function has the form

$$\psi_{q\lambda\mu}=R_{q\lambda}(r)Y_{\lambda\mu}(\theta,\phi) , \quad (11)$$

where $R_{q\lambda}(r)$ is the radial part of the wave function normalized according to

$$\int R_{q\lambda}(r)R_{q'\lambda}(r)r^2dr=\delta(q-q') , \quad (12)$$

and $Y_{\lambda\mu}(\theta,\phi)$ is the μth component of the spherical harmonic with rank λ.

The photoionization rate out of a given sublevel depends on the polarization of the ionizing laser. It is convenient and more general to discuss a cross section that is independent of magnetic sublevel as well as the polarization of the ionizing light. Hence, most treatments of photoionization define an effective cross section for a level as an average of the cross section over the initial-state sublevels and a sum over photon polarizations. An expression for the effective cross section can be derived[17]

$$\sigma=\frac{4\pi}{3}\frac{m_e}{\hbar^2}\frac{k}{q}\frac{1}{g_b}\sum_{a,b,\lambda,\mu,m_s}|\langle b|\mathbf{D}|aq\lambda\mu m_s\rangle|^2 , \quad (13)$$

where g_b refers to the degeneracy of the initial excited state. This cross section is *not* the one generally measured by most experiments because it assumes all initial-state sublevels were equally populated. Most previous experimental cross sections were determined by measuring the number of photoelectrons N_e produced as a function of the ionizing laser fluence F. By monitoring the linear part of the N_e versus F curve, or by fitting a saturation function

$$N_e=N_0\left[1-\exp\left[-\frac{\sigma}{h\nu}F\right]\right] \quad (14)$$

to the experimental results, σ is deduced. However, the cross section measured by these techniques is identical to

the effective cross section σ defined by (13) *only* in the case where all initial sublevels are equally populated. In fact, a cross section measured by such techniques is actually an average of the sublevel cross sections with unknown weights (the initial sublevel populations). A way to circumvent this difficulty is to orient the polarization of the photoionization laser at the magic angle, $\theta_m = 54.7°$, with respect to the experimental axis of quantization. This provides a laser beam with equal components of σ_+-, σ_--, and π-polarized light (see Fig. 3). Then the ionization probability is the same for each magnetic sublevel. To see this, note that in terms of π (polarization along $\hat{\mathbf{z}}$), $\hat{\sigma}_+$, $\hat{\sigma}_-$ components the polarization vector of light oriented at the magic angle in the x-z plane can be written

$$\hat{\epsilon} = \frac{\hat{\mathbf{z}}}{3^{1/2}} + \frac{\hat{\sigma}_- - \hat{\sigma}_+}{3^{1/2}} , \tag{15}$$

where the unit vectors for right- and left-circularly-polarized light are defined by

$$\hat{\sigma}_\pm = \frac{\hat{\mathbf{x}} \pm i\hat{\mathbf{y}}}{\mp 2^{1/2}} . \tag{16}$$

The factor in σ that depends on sublevel is the dipole matrix element [see (10)] and for a given initial sublevel m this factor is

$$\sum_{J',m'} |\langle J'm'|\mathbf{r}_i \cdot \hat{\epsilon}|Jm\rangle|^2 \equiv Q , \tag{17}$$

where the primed quantities correspond to final-state quantum numbers and we have expressed the relevant matrix elements from (10) in terms of eigenstates of the operators $\mathbf{J}$ and J_z. Substituting (15) into (17) and using the Wigner-Eckart theorem gives the result

$$\begin{aligned} Q &= \sum_{J',m'} (|\langle J1m0|J'm'\rangle|^2 + |\langle J1m-1|J'm'\rangle|^2 \\ &\quad + |\langle J1m1|J'm'\rangle|^2) \frac{|\langle J\|r^1\|J'\rangle|^2}{3(2J+1)^{1/2}} \\ &= \frac{1}{3(2J+1)^{1/2}} \sum_{J'} |\langle J\|r^1\|J'\rangle|^2 \\ &\quad \times \sum_{m',q} |\langle J1mq|J'm'\rangle|^2 . \end{aligned} \tag{18}$$

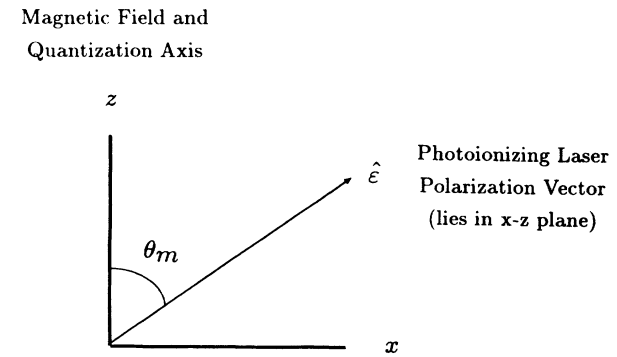

FIG. 3. Linearly polarized light at the magic angle with respect to the quantization axis—the axis of the applied magnetic field.

Then, by applying the Clebsch-Gordan orthogonality relation

$$\sum_{m',q} |\langle J1mq|J'm'\rangle|^2 = \frac{1}{2J'+1} , \tag{19}$$

it is easy to see that (18) is independent of the initial-magnetic-sublevel quantum number m. Hence, the transition rate is the same for each sublevel, and the σ we measure in (8) and the effective cross section given in (13) are identical.

The second important experimental consideration is the choice of direction and polarization of the observed fluorescence. This choice is significant because it determines which sublevel (or which weighted combination of sublevels) one is observing the fluorescence from. It is important to make this choice wisely. A concrete example will show why. Consider the observation of fluorescence from a $J = \frac{3}{2}$ level (e.g., Cs $7D_{3/2} \rightarrow 6P_{1/2}$ line). Assume the initial populations of the upper sublevels are

$$N_1 = N_{\pm 3/2}, \quad N_2 = N_{\pm 1/2} , \tag{20}$$

with $N_{\text{tot}} = 2(N_1 + N_2)$ (refer to Fig. 4). If we choose to observe π fluorescence then the signal S depends only on the population of the $m_j = \pm\frac{1}{2}$ sublevels, i.e.,

$$S \propto N_2 . \tag{21}$$

This is unacceptable because the same laser that photoionizes the excited atoms could produce coherent effects that redistribute the population among magnetic sublevels.[18] Such effects can be very pronounced depending on the laser intensity, its detuning from allowed transitions, and the oscillator strengths of these transitions. This problem can be circumvented by observing fluorescence (1) at right angles to the quantization axis, and (2) with polarization at $\theta_m = 54.7°$ to the quantization axis.

Our discussion of the need for these conditions begins by expressing the initial excited-state density operator ρ_0 with irreducible tensor basis operators

$$\rho_0 = \sum_{L,M} a_{LM} T_{LM} , \tag{22}$$

where T_{LM} is the Mth component of a spherical tensor of

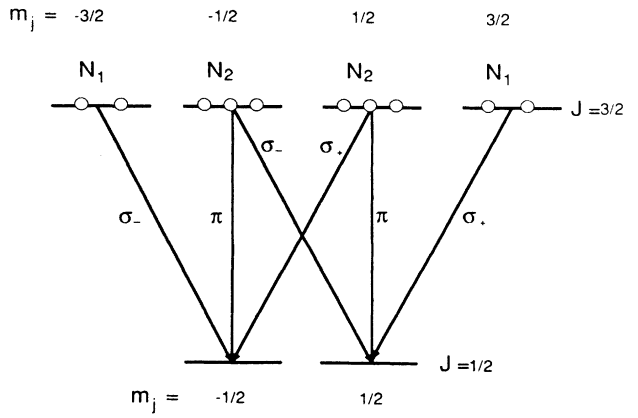

FIG. 4. Components of fluorescence produced by sublevel transitions of the Cs $7D_{3/2} \rightarrow 6P_{1/2}$ line ($\lambda = 672$ nm).

rank L and a_{LM} is the corresponding amplitude of this tensor in the initial populations distribution. The tensor T_{LM} is defined to be

$$T_{LM}=\sum_m |Jm\rangle\langle Jm-M|(-1)^{m-M-J} \times C(J,J,L;m,M-m)\ , \tag{23}$$

where $C(J,J,L;m,M-m)$ is a Clebsch-Gordan coefficient. We note that, physically, the presence of T_{LM} components where $L\neq 0$ in the initial density operator ρ_0 represent contributions depending on sublevel population differences or anisotropies. An isotropic or uniform population distribution is expressed by the term $a_{00}T_{00}$ in the density operator. The photoionization laser can, under the right conditions, cause a significant redistribution of magnetic sublevel population. This causes the final density operator (after the second laser pulse has ended) to have the same form as (22) but with different (and time-dependent) coefficients.

It can be shown that the subsequent power of fluorescence propagating at right angles to the quantization axis and linearly polarized along the unit vector $\hat{\mathbf{u}}$ (see Fig. 5) is given by[18]

$$P(\hat{\mathbf{u}})=Ne^{-t/\tau}\left[K_0+K_2\sum_M e^{-iM\Omega t}Y_{2M}(\hat{\mathbf{u}})V^{22}_{M0}\right]\ , \tag{24}$$

where K_0 and K_2 are constants and the matrices V^{22}_{MN} (discussed in the work of van Wijngaarden *et al.*[18]) represent sums over products of Clebsch-Gordan coefficients and Wigner d matrices. The quantity Ω is the electronic polarization precession frequency defined by

$$\Omega=\frac{g_J\mu_B B+A_J m_I}{\hbar}\ , \tag{25}$$

where m_I is the projection of the nuclear spin on the z axis, A_J is the magnetic dipole hyperfine constant, g_J is the electronic g factor of the initial level, μ_B is the Bohr magneton, and B is the applied magnetic field. The magnetic field must be large enough to make J a reasonably good quantum number and must be applied along the quantization axis. This means that $g_J\mu_B B \gg A_J m_I$ and that (25) can be expressed as $\Omega\simeq g_j\mu_B B/\hbar$. The magnetic field causes the Y_{2M} ($M\neq 0$) terms in the *integrated* fluorescence signal [integral of (24) over several lifetimes] to be reduced by at least $1/\Omega\tau$ compared to the Y_{20} term.[18] If we can neglect $Y_{2M}(M\neq 0)$ terms compared to the Y_{20} term ($\Omega\tau\gg 1$), then the integrated fluorescence signal has the following dependence on polarization angle θ (see Fig. 5) and sublevel populations:

$$S\propto\int_{t_0'}^{t_0'+3\tau}P(\hat{\mathbf{u}})dt\propto\tau N[K_0+K_2Y_{20}(0,\theta)V^{22}_{00}]\ . \tag{26}$$

Expressing this result in simpler form, we have

$$S=b_0+b_2P_2(\cos\theta)\ , \tag{27}$$

where

$$P_2(x)=\tfrac{1}{2}(3x^2-1) \tag{28}$$

is the second-order Legendre polynomial and b_0 and b_2 are constants. Note we have used the relation $Y_{20}(\phi,\theta)\propto P_2(\cos\theta)$. Thus, by choosing $\theta=\theta_m$ where $P_2(\cos\theta)=0$, the term in the signal that depends on population differences vanishes. This is the term that may vary due to coherences. In this case the signal only depends on the total population, regardless of the properties of the photoionizing laser. We point out that the magnetic field B required to satisfy the condition $\Omega\tau\gg 1$ is usually rather modest ($B\lesssim 100$ G).

The third important point is that lasers generally have inhomogeneities and hot spots unless special care is taken to produce a uniform beam, viz., spatial filtering. Since different fluences will be present in different parts of the laser beam, atoms in different parts of the beam will have different ionization probabilities. To account for this it is necessary to weigh the ionization probability at a given fluence by the probability of that fluence and then integrate over all fluences. Thus, it is necessary to know something about the fluence probability distribution of the laser beam. The laser beam is somewhat speckled due to the index inhomogeneities in the dye used to generate the light. Inhomogeneities in the optical elements used to guide and steer the beam around the laboratory also contribute to speckling. Thus the most natural fluence probability density function to use for the fluence distribution is that for speckle. To further ensure the laser is properly speckled, we send it through a random-phase plate that forces the beam to have a speckle distribution. The statistics of speckle is well known[19] and the probability of having a fluence between F and $F+dF$ is

$$P(F)dF=\exp\left[-\frac{F}{F_0}\right]\frac{dF}{F_0}\ , \tag{29}$$

where F_0 is the mean fluence of the distribution. Multiplying the signal at a given fluence [see (8)] by this distri-

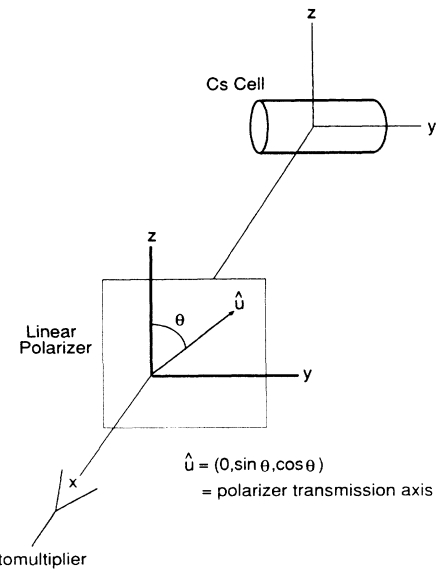

FIG. 5. Fluorescence detection scheme showing the linear polarization required for the signal to be independent of excited-state sublevel population differences.

bution and integrating over all fluences yields the result

$$R(F_0) \equiv \int_0^\infty R(F)P(F)dF$$
$$= \int_0^\infty A_0 \exp\left[-\frac{F}{F_*}\right] \exp\left[-\frac{F}{F_0}\right] \frac{dF}{F_0}$$
$$= \frac{A_0}{1+F_0/F_*} , \tag{30}$$

where

$$F_* \equiv \frac{h\nu}{\sigma} . \tag{31}$$

We fit this function to our data. Again there is only one adjustable parameter—the cross section σ.

III. EXPERIMENT

An energy-level diagram showing the various physical processes that are utilized in Cs is given in Fig. 1. Our experimental setup is sketched in Fig. 6. Two dye lasers pumped by the second harmonic of a Nd:YAG (YAG denotes yttrium aluminum garnet) laser are generally used—one for excitation and one for photoionization. Both dye lasers had similar temporal widths ($\Delta t \simeq 3$ ns). Obviously, for the photoionization measurements at 532 and 1060 nm we used the second harmonic and the fundamental of the Nd:YAG laser as the photoionizing beams. Both of these also had pulsewidths that were very short ($\Delta t \lesssim 4$ ns). The Cs target consisted of a cylindrical glass cell evacuated to 10^{-6} Torr and loaded with about a gram of Cs. The cell is housed in a larger cylindrical glass tube that is heated to 70 °C. At this temperature the Cs number density is 3×10^{12} cm^{-3}. The first dye laser produces light at 767 nm that corresponds to the $6S_{1/2} \rightarrow 7D_{3/2}$ two-photon resonance in Cs. The light is vertically polarized and defines our axis of quantization.

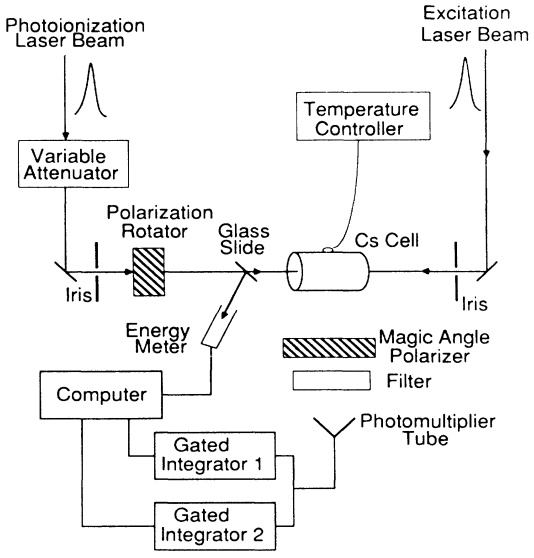

FIG. 6. Experimental setup. The Cs cell was placed between a pair of Helmholtz coils (not shown).

A 60-G magnetic field is applied along the quantization axis in order to decouple the nuclear spin from the electronic spin in the excited $7D_{3/2}$ level and to allow us to ignore population differences that provide T_{2M} terms in our fluorescent power [see (24)]. The second dye laser is delayed with respect to the first by having it traverse a longer path. This dye laser is used for photoionization. In order to allow us to vary its fluence this laser is sent through a variable attenuator. It is polarized at an angle $\theta_m = 54.7°$ to the quantization axis for reasons discussed in the previous section. This angle of polarization is produced by sending the light through a commercial polarization rotator (a Fresnel rhomb). This laser is passed through a random-phase plate[20] and a weak lens before it enters the cell. The purpose of this is to provide an intensity distribution in the cell that is statistically well characterized as discussed in the last section. We also pick off a small portion of this laser's energy (typically about 8%) and send it to an energy meter whose signal is then read and stored by a personal computer. Fluorescence produced by the spontaneous decay of the $7D_{3/2}$ level to the $6P_{1/2}$ level at $\lambda = 672$ nm is detected by a photomultiplier tube (PMT) after the fluorescence has passed through a sheet of polaroid and a narrowband filter [full width at half maximum (FWHM) bandwidth of 10 nm]. The polaroid is oriented at the angle θ_m to the quantization axis to ensure that our signal is proportional to the total number of excited atoms. The PMT signal is amplified using a wide bandwidth low-noise amplifier and then the signal is split and sent to two gated integrators that will integrate different temporal portions of the fluorescence decay curve. The output signals of the two integrators are then read and stored by a computer.

We measured the mean lifetime of a cesium atom in the $7D_{3/2}$ level to be 100 ns. The measurement was made with a fast Tektronix transient digitizer. The delay between the excitation laser pulse and the photoionization laser pulse was typically 25 ns. The integration times of the two gates were set as follows: the first integrator, which integrated fluorescence before the photoionization pulse, was set to integrate for $T_1 = 15$ ns; the second integrator started integrating just after the photoionization pulse ended ($t \simeq 30$ns) and integrated for $T_2 = 250$ ns.

For each laser pulse we recorded the two fluorescence signals sent from the gated integrators and we recorded a fraction of the photoionizing laser's energy using a commercial pyroelectric energy meter. The ratio of the two fluorescence signals was subsequently calculated, the data was binned according to energy, and then all the values of the ratios were averaged for a given energy bin. The energy axis was split into 250 points. The total number of raw data points for a given run was 7000. Thus, each energy bin reflects an average over roughly 28 raw ratio data points. After processing, the data consisted of the fluorescence ratio and the corresponding energy (chosen as the midpoint of the appropriate bin). The energies were converted to fluences by dividing by the area of the excitation beam $A_{exc} = 0.15$ cm^2. The excitation beam area was well defined by sending it through an aperture. The photoionization beam area was kept larger than the excitation beam area. The area A_{exc} was accurately mea-

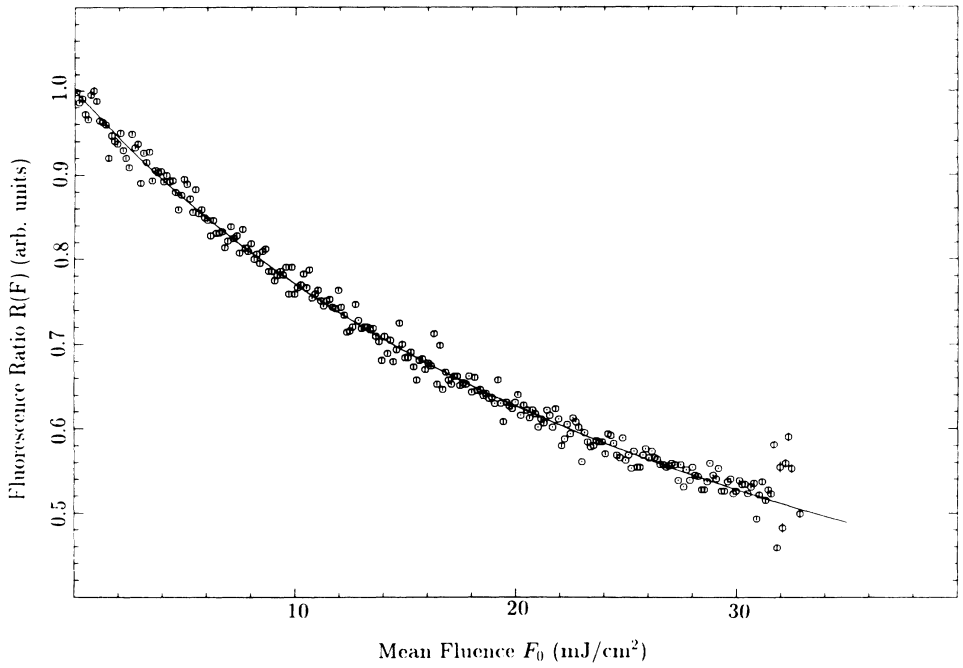

FIG. 7. A plot of the fluorescence ratio vs photoionization fluence F_0. The photoionization laser wavelength was $\lambda_2 = 700$ nm. Included on the plot is a fitted curve [see (30)] with one free parameter of value $F_* = 33.4$ mJ/cm^2.

sured using a charged-coupled device (CCD) array and a frame grabber. The frame grabber is a plug-in board for our laboratory personal computer. It can store two images each consisting of 512×480 pixels. Each pixel has area $\simeq 209$ μm^2; the intensity resolution is 8 bits. The beam area was found by integrating the image over a circle centered on the laser beam and varying the circle's radius until the integrated signal was about 97% of the total integral for the image.

We also analyzed the fluence distribution of the photoionization beam using a CCD array and a frame grabber. The dye-laser-fluence distribution was close to that of a fully speckled beam. However, the fundamental YAG-laser-fluence distribution was not fully speckled but had a distribution between a speckle pattern and a uniform beam. This also manifested itself in visibly poorer fits to the ratio-versus-energy data when a speckle distribution was assumed. In this case we numerically fit the fluorescence ratio-versus-fluence curve using the fluence-distribution data measured using the CCD array. It should be mentioned that we had to use a second, different Nd:YAG laser to get the 1060-nm data. This is because the output from the first YAG laser was elliptically polarized as a result of second-harmonic generation (used to pump the excitation dye laser). Thus, in order to get clean, vertically polarized YAG light a second YAG unit was borrowed.

It is important to avoid overpopulating the excited level to the point where superfluorescent effects occur. There are a number of lower-lying levels to which superfluorescence might be possible (e.g., $8P$, $4F$, $7P$). In fact at large excitation beam fluences, $F_{\rm exc} \gtrsim 50$ mJ/cm^2, we observed a fluorescence-decay curve that had a pro-

TABLE I. Photoionization cross sections for the $7D_{3/2}$ state of Cs.

λ (nm)	$h\nu$ (eV)	σ (Mb)[a]
1060	1.16	12.8
867	1.43	11.8
700	1.77	8.7
641	1.94	8.6
588	2.11	5.3
532	2.33	3.1

[a]1 Mb $= 10^{-18}$ cm^2.

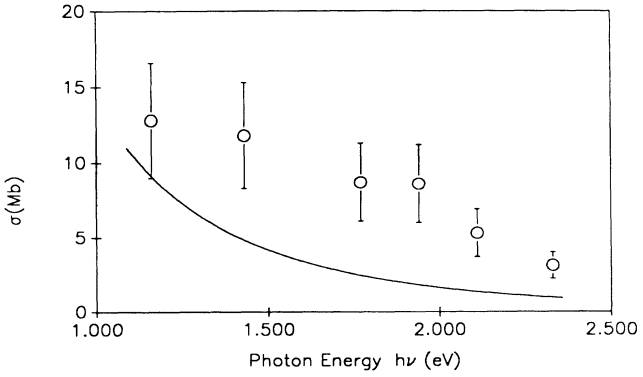

FIG. 8. A plot of the photoionization cross section of the Cs $7D_{3/2}$ level measured at six different photon energies. The solid curve represents the result of a quantum-defect theory calculation of the photoionization cross section.

nounced peak at the beginning with a steep falloff (width $\simeq 15$ ns) and then the typical exponential decay thereafter. This type of behavior is at least indicative of superfluorescence—where a rapid depopulation occurs until the upper and lower levels become equal and then the upper level resumes its normal spontaneous decay. We did not investigate this further except to ensure that we operated at excitation intensity levels well below the onset threshold for this phenomenon. We also checked that the fluorescence depended quadratically on excitation intensity as expected in the low-signal limit for a two-photon process.

IV. RESULTS AND DISCUSSION

A typical set of data is shown in Fig. 7. This plot also includes a fitted curve that corresponds to the function expected in the case of a fully speckled photoionization pulse [see (30)]. The only parameter that is allowed to vary is the cross section [actually the related quantity F_*, see (31)].

The results are summarized in Table I. The error bars of 30% are estimates based on the uncertainties involved in our measurements and fits. Contributions to uncertainties include the energy (5%), the beam area (3%), fluorescence ratio (10%), and the photoionization-laser-fluence distribution (25%).

Since no other measurements for the photoionization cross section of this level have been reported in the literature, we cannot compare our measurements with previous results. However, the cross-section measurements of Gerwert and Kollath[8] for the Cs $6D_{3/2}$ level are qualitatively similar to those reported here. They measured cross sections at 13 different wavelengths in the range 420–580 nm. Their values seemed to be relatively constant, fluctuating between 10–30 Mb.

A plot of our data, in terms of cross section versus photon energy, is provided in Fig. 8. Although there are no theoretical calculations of the Cs $7D_{3/2}$ photoionization cross sections in the literature, we have calculated cross-section values using expressions derived from a quantum-defect-theory (QDT) analysis made by Burgess and Seaton.[21] The solid line in Fig. 8 corresponds to the results of such a calculation. From the figure it is clear that our measurements show a general decrease in cross section with photon energy—in qualitative agreement with the quantum-defect-calculation results. However, the measured cross-section values are about a factor of 3 higher than the calculated values. In a similar comparison between cross-section measurements made on the Cs $7P_{3/2}$ level by Gerwert and Kollath[8] and QDT calculated cross sections, the measured values were about a factor of 2 higher than those which were calculated (see also Wuilleumier[10]).

V. CONCLUSIONS

We developed a technique to deduce excited-state photoionization cross sections σ from a measurement of two integrated fluorescent signals. The ratio of the two integrated fluorescent signals is proportional to $\exp(-F\sigma/h\nu)$ in the case of a uniform laser beam or to $(1+F\sigma/h\nu)^{-1}$ in the case of a speckled beam, where F is the fluence (energy per area) of the photoionizing laser pulse, and $h\nu$ is the energy of a photon. By varying the fluence F, a photoionization curve can be generated that can be fit to the function above with only one free parameter, σ. It is important that both the ionizing laser polarization and the measured fluorescence polarization be at the magic angle ($\theta_m = 54.7°$) with respect to the quantization axis. In the former case, this ensures that the ionization probability is independent of magnetic quantum number sublevel. In the latter case, it ensures that the observed fluorescence is proportional to the total number of excited atoms in all magnetic sublevels. For these polarizations, significant changes in the distribution of magnetic sublevels that occur under many experimental conditions are unimportant and will not affect the final result. We applied the technique to the $7D_{3/2}$ level of Cs and determined photoionization cross sections at six different wavelengths.

Finally, we stress the simplicity of our method: it requires a simple enclosed cell with no need for an expensive and cumbersome vacuum system; it relies on the straightforward measurement of fluorescence using a single photomultiplier tube and a pair of inexpensive gated integrators; the data is easily fit to a simple function determined by a choice of laser-fluence distribution. The result is an accurate but simple measurement of the absolute photoionization cross section of an excited atomic state.

ACKNOWLEDGMENTS

We thank Will Happer for his support, encouragement, and especially for a critical reading of the manuscript. Our work also greatly benefitted from discussions with Thad Walker. Bob Austin is to be thanked for the use of his YAG laser. We are grateful for the support of the Department of Energy under Contract No. LLNL-DOE S-C1133303 and we also thank the Army Research Office for their support under Contract No. DAAL-87-K-0068.

[1] A. Z. Msezane and S. T. Manson, Phys. Rev. Lett. **35**, 364 (1975).
[2] A. Z. Msezane and S. T. Manson, Phys. Rev. Lett. **48**, 473 (1982).
[3] J. Lahiri and S. T. Manson, Phys. Rev. Lett. **35**, 614 (1982).
[4] H. P. Saha, M. S. Pindzola, and R. N. Compton, Phys. Rev. A **38**, 128 (1988).
[5] R. V. Ambartzumian, N. P. Furzikov, V. S. Letokhov, and A. A. Purtesky, Appl. Phys. **9**, 335 (1976).
[6] U. Heinzmann, D. Schinkowski, and H. D. Zeman, Appl. Phys. **12**, 113 (1977).
[7] A. V. Smith, J. E. M. Goldsmith, D. E. Nitz, and S. J. Smith, Phys. Rev. A **22**, 577 (1980).
[8] K. Gerwert and K. J. Kollath, J. Phys. B **16**, L217 (1983).

[9]S. L. Gilbert, M. C. Noecker, and C. E. Wieman, Phys. Rev. A **29**, 3150 (1984).
[10]F. J. Wuilleumier, D. L. Ederer, and J. L. Picque, in *Advances in Atomic and Molecular Physics*, edited by D. Bates and B. Bederson (Academic, New York, 1988), Vol. 23, pp. 197–286.
[11]V. L. Jacobs, J. Phys. B **5**, 2257 (1972).
[12]J. Kessler, *Polarized Electrons*, 2nd ed. (Springer-Verlag, New York, 1984), pp. 144–165.
[13]N. B. Avdonina and M. Ya. Amusia, J. Phys. B **16**, L543 (1983).
[14]J. Lahiri and S. T. Manson, in *Abstracts of Contributed Papers*, Proceedings of the Twelfth International Conference on Physics of Electronic and Atomic Collisions, edited by S. Datz (U.S. AEC, Gatlinburg, Tennessee, 1981), p. 39.
[15]A. Z. Msezane and S. T. Manson, Phys. Rev. A **29**, 1594 (1984).
[16]J. K. Sprong, J. D. Kmetec, S. C. Wallace, J. F. Young, and S. E. Harris, Phys. Rev. Lett. **58**, 2631 (1987); S. E. Harris, Opt. News **41**, 11 (1988).
[17]I. I. Sobleman, *Introduction to the Theory of Atomic Spectra* (Pergamon, New York, 1972), pp. 353–376.
[18]W. A. van Wijngaarden *et al.*, Phys. Rev. Lett. **56**, 2024 (1986); W. A. van Wijngaarden, K. D. Bonin, and W. Happer, Phys. Rev. A **36**, 1187 (1987).
[19]J. Goodman, in *Laser Speckle and Related Phenomena*, edited by J. C. Dainty (Springer-Verlag, New York, 1984), pp. 9–75.
[20]K. D. Bonin and M. Kadar-Kallen (unpublished).
[21]A. Burgess and M. Seaton, Mon. Not. R. Astron. Soc. **120**, 121 (1960).